Modulating the transport property of flexible $La_{0.67}Ca_{0.33}MnO_3$ thin film by Mechanical bending

Wentao Hua,[1] Lu Lu,[2] Lvkang Shen,[2] Jing Jin,[2] He Wang,[2] Ming Liu,[2]

Chunrui Ma,[1*] Chun-Lin Jia[2,3]

[1]*State Key Laboratory for Mechanical Behaviour of Materials and School of Materials Science and Engineering, Xi'an Jiaotong University, Xi'an, 710049, China*

[2]*School of Microelectronics, Xi'an Jiaotong University, Xi'an 710049, China*
[3]*Ernst Ruska Centre for Microscopy and Spectroscopy with Electrons, Forschungszentrum Jülich, D-52425 Jülich, Germany*

Flexible epitaxial $La_{0.67}Ca_{0.33}MnO_3$ (LCMO) thin films are fabricated on $SrTiO_3$ buffered (001)-oriented fluorophlogopite substrate. The metal-to-insulator transition tends toward lower temperature when subjecting to mechanical bending. Moreover, the transport behavior of the bent LCMO films in the insulating region follows variable Range hopping model and the resistivity increases with reduction of the bending curvature radii because the applied strain aggravates the distortion of LCMO crystal structure, decreases hopping distance and hence impedes the transport of charge carrier. The resistivity change induced by the mechanical bending can go up to 10^4 % at 100 K and 10^5 % at 10 K. Such large resistivity change makes the flexible LCMO thin film promising as a mechanical-bending switch device at low temperature.

* Corresponding authors: chunrui.ma@mail.xjtu.edu.cn;

Thin films of Mixed-valance perovskite manganites $La_{1-x}A_xMnO_3$ (A = Sr, Ca, Ba) have attracted worldwide attention due to the abundant distinct physical phenomena, such as colossal magnetoresistance effect, the transition from paramagnetic to the ferromagnetic state, the metal to insulator transition (MIT), phase separation and so on.[1-4] These ponderable physical mechanisms make it potentially applicable in the area of magnetic random-access memories, magnetoelectric devices, tunneling magnetoresistance devices and switching devices.[5-7] Among these materials, $La_{0.67}Ca_{0.33}MnO_3$ (LCMO) has become one of the mostly invested materials due to its complex pattern of spin, orbital, charge and Jahn-Teller lattice distortions,[8-10] which induces a variety of exotic phenomena, such as huge magnetoresistance effect. Moreover, as the representative of narrow bandwidth manganites with robust Jahn-Teller coupling, its electrical transport is very sensitive to the external environment and exhibits various novel physical phenomena.[11-12] A small external perturbation can influence the Mn^{3+}/Mn^{4+} exchange effect[13] and the Jahn-Teller distortion,[14] and thus generate a large change in transport properties. So far, many researchers have devoted efforts to investigate the effect of the external strain on its physical mechanism. One way was to take advantage of lattice mismatch between the film and substrate to build various interface strain.[15,16] For example, Helali *et al* fabricated LCMO on $LaAlO_3$, $SrTiO_3$ and $(LaAlO_3)_{0.3}$-$(SrAlTaO_6)_{0.7}$ to generate compressive strain, tensile strain and negligible tensile strain, respectively. It is found that both tensile and compressive strain can increase the thermal activation energy and the variable Range hopping (VRH) characteristic temperature in the paramagnetic

state.[17] Another way to study the strain effect on transport behavior was to fabricate several samples with different thickness, since the interface strain induced by the lattice mismatch between the film and substrate is gradually released by formation of dislocation or defects with the increasing film thickness.[18,19] Gao *et al* found that a dead layer about 6 nm thickness was formed in LCMO epitaxial thin films and the conductivity of the films was linearly increased with the film thickness due to the reduced effects of the dead layer.[20] However, the properties of the films are not only affected by strain, but also by the microstructure induced by different growth modes and by crystalline quality on different substrates. Therefore, it is necessary to find a way to explore the influences of pure strain on the film properties.

Flexible thin film is not only the basis of wearable/portable electronic devices, but also provides a test sample for modulating or exploring the novel physical properties by applying stretching strain or mechanical bending strain. Until now, two methods have been used to fabricate flexible epitaxial function oxide thin films. One is to transfer the desired thin film from a rigid substrate to a flexible substrate through etching a buffer layer between the desired thin film and the rigid substrate.[20] Another is to directly fabricate the desired thin film on flexible mica substrate.[21] Recently, Hong *et al* investigated the effect of extreme tensile strain on $La_{0.7}Ca_{0.3}MnO_3$ membranes fabricated through transferring epitaxial $La_{0.7}Ca_{0.3}MnO_3$ thin film onto the polyimide sheet, and found that uniaxial and biaxial tensile strain benefits the formation of antiferromagnetic insulating state and suppression of ferromagnetic metal.[22] However, few research was contribute to investigation of the effects of

mechanical bending strain on the transport properties of the LCMO thin films. Comparing to transferring method, the direct fabrication method can effectively avoid the contamination induced during the transferring process.

In the present paper, the flexible epitaxial (111) LCMO thin films were fabricated the STO-buffered (001) fluorophlogopite single-crystalline substrates (F-Mica). The effects of mechanical bending strain on the transport properties of the LCMO thin films were explored with and without magnetic field.

For preparation of the flexible epitaxial LCMO thin films, an epitaxial STO buffer layer was first deposited on the (001) F-Mica substrate at an oxygen pressure of 50 mTorr via 248 nm KrF excimer pulsed laser deposition (PLD) system with the laser energy of 500 mJ. Then, the oxygen pressure and the laser energy were increased to 250 mTorr and 650 mJ to grow the LCMO thin film on top of the STO buffer layer. The repetition rate of laser was fixed at 5 Hz for the growth of both STO and LCMO. After deposition, the thin films were annealed at 1000 ℃ for 15 mins at oxygen pressure of 200 Torr and then cooled down to room temperature at a rate of 25 ℃ per min. The crystallinity and quality of the epitaxial LCMO thin films were characterized by high-resolution X-ray diffraction (HRXRD) using the PANalytical X'Pert MRD system. Reciprocal space mappings (RSM) were conducted to determine the crystal structure by using the scanning line detector. The microstructure of the films was investigated by transmission electron microscopy (TEM). The transport properties were measured by Van der Pauw method with the physical property measurement system (PPMS). The flexible film/F-Mica was peeled off mechanically

from the substrate bulk with the assist of polyimide type. The bending states of the LCMO thin films were realized by attaching the films to an insulating double-faced adhesive tape on the copper molds with the bending curvature radii of 25 mm, 12.5 mm and 7.5 mm.

Figure 1(a) shows the XRD θ-2θ scanning pattern of the LCMO and STO thin film system on F-Mica substrate. Only the (111) and (222) peaks of LCMO and STO and the {00l} peaks of F-mica can be seen, showing that the films grow with the {111} atomic planes parallel to the (001) plane of the F-Mica substrate. In order to investigate the in-plane orientation relationship between the film and the F-Mica substrate, φ scans were performed around {002} reflections of STO and LCMO, and {202} reflections of the F-Mica substrate as shown in Figure 1(b). It is clearly seen that the F-Mica peaks show 3-fold symmetry and the films exhibit a 6-fold symmetry, which is indicative of the in-plane relationship of $[1\,\dot{1}\,0]_{LCMO}//[1\,\dot{1}\,0]_{STO}//[010]_{F\text{-}Mica}$. According to the out-of-plane and in-plane orientation relationship between the films and the substrates, it can be derived that the fabricated films are epitaxial. This epitaxial relationship also confirmed by selected-area electron diffraction (SAED) pattern of the sample recorded along the $[1\,\dot{1}\,0]$ zone axis of F-Mica as shown in the inset of Figure 1(c). The thickness of the LCMO and STO layers is around 22 nm and 13 nm, respectively, which were measured from the cross-section TEM image (Figure 1c). From the symmetric RSMs taken around the (111) reflections of the multilayer and the (001) reflection of the F-Mica substrate in Figure 1(d), the (111) plane spacing of the LCMO and STO layers are measured as 2.218 Å and 2.239 Å, respectively. In

comparison with the corresponding (111) plane spacings (2.227 Å for LCMO and 2.255 Å for STO) of bulk materials,[23] the LCMO and STO thin film undergo compressive strain of ~0.40% and ~0.71%, respectively, along the out-of-plane direction. From the asymmetric RSMs taken around the (213) reflections of the LCMO films and the (228) reflections of the F-Mica substrates, as shown in Figure 1(e), a plane spacing of 1.884 Å and 1.887 Å is measured along the in-plane [1 $\bar{1}$ 0] directions, respectively, for the LCMO and STO layers, which is larger than that of the LCMO (1.819 Å) and the STO (1.841 Å) bulk materials, leading to an in-plane tensile strain of ~ 3.57% in the LCMO layer and ~ 2.50% in the STO layer.

Figures 2 (a-b) (Linear scale shown in Figure S2-5) show the data of resistivity measured in a range of temperature from 10 to 350 K at 0 T in tensile and compressive mechanical strain. A normal MIT process occurs for the film at flat state and the transition temperature is about 204 K, which is lower than the value of bulk material (265 K), probably due to in-plane tensile strain of 3.57% induced by lattice mismatch between the films and substrate.[24] The transition temperature tends to lower temperature at mechanical bending state, since the mechanical bending induced tensile and compressive strain is likely to distort the lattices of film and hence hinder the transport of charge carriers in the film, making LCMO goes into insulator state earlier when it is warmed from 10 to 350 K. This phenomenon consists with the Monte Carlo simulation reported by Sen *et al* that LCMO gradually comes into an insulating charge-ordered phase from a charge disordered metallic phase as strain increase.[25] From Figure 2(c), it is can be seen that the MIT temperature increases to

268 K at the flat state, indicating that the magnetic field enhances the double exchange and postpone it to enter into insulator state. However, it is unexpected that the MIT disappear in the test temperature range under the mechanical bending strain as shown in Figure 2(c-d). The abnormal phenomena probably can contribute to the slowly decreasing resistivity with the increase of temperature. It is known that the magnetic field will provide the energy to assist charge carrier to transport in the film and reduce the resistivity of LCMO (Figure S6), while the mechanical bending strain prevent the charge carrier to transport and increase its resistivity. The competition between energy from magnetic field and mechanical bending strain merges MIT. In order to understand the transport mechanism under the effect of extra mechanical strain, the measured resistivity in the high temperature region was simulated using thermal activation model (Figure S7),[23] small-polaron hopping (Figure S8)[26] and VRH model.[27] It is found that the VRH model fits the data very well, as shown in Figure 3, implying that the transport mechanism in the LCMO films is the charge carriers hopping between localized electronic states. In VRH model $\rho(T) = \rho_0 e^{(T_0/T)^{1/4}}$, where T_0 represents a characteristic temperature and is proportional to the slope of a plot of ln(ρ) versus $T^{-1/4}$.[27] It is known that the average nearest-neighbor hopping distance $R = \left[\frac{9}{8\pi\alpha N(E)kT}\right]^{1/4}$ and the localization length $\frac{1}{\alpha}=\left(\frac{171U_m\mathrm{V}}{kT_0}\right)^{1/3}$, where V is the unit-cell volume per Mn ion, k is Boltzmann constant, and U_m=3J_H/2 is the splitting energy between the spin-up and spin-down e_g bands. J_H is coefficient of the Hund's rule coupling and U_m≈2 eV in manganites. $N(E)$ is the available density states, where the charge carrier can hop to. Based on the calculation of Viret *et al*, the $N(E)$ is

around 9×10^{26} $m^{-3}eV^{-1}$.[26] Here, we assume the volume of unit-cell conservation under the strain. Hence, the hopping distance can be obtained and is summarized in in Table 1 with the fit value of T_0. It is found that hopping distance decreases with the increase of mechanical bending strain, no matter tensile or compressive strain, except the compressive strain of 0.8%, which is slightly larger than the value of the compressive strain of 0.4%. T_0 exhibits the opposite trend to hopping distance. It is known that T_0 is proportional to the hopping energy from one localized state to another.[28.29] The reduction of hopping distance and the increased hopping energy indicate that the applied strain aggravates the distortion of LCMO crystal structure and impede the transport of charge carrier and enhance its insulator behavior.[22]

Figure 4 exhibits the resistivity change ratio $(\rho_{bent}-\rho_{flat})/\rho_{flat}\times100\%$, where ρ_{bent}, ρ_{flat} is the resistivity of the film at bending and flat state, as function of temperature from 10 to 200 K with and without magnetic field. It is found that the resistivity change ratio increases from ~10^2 % at 200 K to ~10^4 % at 100 K, then it slowly increases to ~10^5 % at 50 K and almost remains unchanged until to10 K. The change ratio is even higher with the application of magnetic field. As shown in Figure 2, the huge resistivity change without/with magnetic field can contribute to the different scenario of $\rho(T)$ at low temperature. The LCMO thin film stays a metallic state in the absent of extra mechanical strain, while the application of mechanical strain triggers an insulating state. As Sen *et al* 's calculation based on Monte Carlo simulation, there is a transition in LCMO from a metallic ground state at small strain to an insulating state at large strain.[25] That is to say, as the increased strain, the

Jahn-Teller distortion drives double-exchange induced metallic state gradually to become a charge-ordered insulating state. Therefore, the suppressed ferromagnetic metallic phase and the activation of charge-ordered insulating state under the mechanical strain promotes this huge resistivity change. If the flat state with low resistivity is set as "on" state, the bending state with large resistivity is set as "off" state. The resistivity change shows the huge change from the metal state to the insulator state in the LCMO thin films through the mechanical bending. High sensitivity makes our designed LCMO thin films promising for application in flexible resistivity switch at low temperature.

In conclusion, flexible epitaxial (111)-oriented LCMO thin films with STO buffer layers were fabricated on F-Mica substrate using pulsed laser deposition system. Both extra tensile and compressive mechanical strain induce the MIT peaks of LCMO become subtle and the transition temperature turns to lower temperature. Although the applied magnetic field provides energy to excite the charge carrier hopping and increases the MIT temperature, the energy is still not enough to overcome electron localization and thus the film exhibits insulator behavior at low temperature. The resistivity change by extra strain can go up to at least 10^5 % relative to that of no extra strain at 50 K, since Jahn-Teller distortion tends to be enhanced by the extra mechanical tensile or compressive strain in LCMO thin film. This huge resistivity change at low temperature suggests that the designed flexible LCMO thin film can be used as bending-induced resistivity switch at low temperature.

Supplementary Material

See the Supplementary Material for the bending strain calculation, details for transport properties under mechanical tensile and compressive strain in the linear coordinate system and the thermal activation and small-polaron hopping model data fitting.

Acknowledgments

This research is supported by the Natural Science Foundation of China (nos. 51702255 and 51390472), the National “973” projects of China (nos. 2015CB654903, 2015CB654603), the Shaanxi Natural Science Foundation 2018JM5069, and the Fundamental Research Funds for the Central Universities.

Data Availability

The data that support the findings of this study are available from the corresponding author upon reasonable request.

References:

[1] S. Jin, T. H. Tiefel, M. McCormack, R. A. Fastnacht, R. Ramesh, and L.H. Chen Science **264,** 413-415 (1994).

[2] R. von Helmolt, J. Wecker, B. Holzapfel, L. Schultz, and K. Samwer, Phys. Rev. Lett. **71,** 2331-2334 (1993).

[3] M. A. Subramanian, B. H. Toby, A.P. Ramirez, W. J. Marshall, A.W. Sleight, and G. H. Kwei, Science **273,** 81-84 (1996).

[4] A. S. McLeod, Jingdi Zhang, M. Q. Gu, F. Jin, G. Zhang, K. W. Post, X. G. Zhao, A. J. Millis, W. B. Wu, J. M. Rondinelli, and et al, Nat Mater **19,** 397-404 (2020).

[5] Yu Lu, X. W. Li, G. Q, X. Gang, and Gang Xiao, Phys. Rev. B **54**, R8357 (1996).

[6] T. Sun, J. Jiang, Q.M. Chen, and X. Liu, Ceram. Int. **44**, 9865-9874 (2018).

[7] M. Viret, J. Nassar, M. Drouer, J. Contour, C. Fermon, and A. Fert, J. Magn. Magn. Mater. **198-199**,1-5 (1999).

[8] Z. Guo, D. Lan, L.L. Qu, K.X. Zhang, F. Jin, B.B. Chen, S.W. Jin, G.Y. Gao, F. Chen, L.F. Wang, and et al, Appl. Phys. Lett. **113,** 231601 (2018).

[9] Kalipada Das, and I. Das, J. Appl. Phys **121,** 103904 (2017).

[10] M. Fath, S. Freisem, A. A. Menovsky, Y. Tomioks, J. Aarts, and J. A. Mydosh, Science 285,1540-1542 (1999).

[11] W. W. Gao, F. X. Hu, B. G. Shen, and J. R. Sun, J. Appl. Phys **117,** 17C733(2015).

[12] M. Navasery, S. A. Halim, A. Dehzangi, N. Soltani, G. Bahmanrokh, M. Erfani H, A. Kanalianfar, K. Y. Pan, S. C. Chang, S. K. Chen, and et al, Appl. Phys. A **116,**

1661-1668 (2014).

[13] K. Kawashima, G. Logvenov, G. Christiani, and HU. Habermeier, J. Magn, Magn, Mater. **378,** 539-545 (2015).

[14] B. B. Chen, P. F. Chen, H. R. Xu, X. L. Tan, F. Jin, Z. Guo, B. W. Zhi, and W. B. Wu, Appl. Phys. Lett. **104,** 242416 (2014).

[15] Sujit Das, Andreas Herklotz, Er Jia Guo, and Kathrin Dorr, J. Appl. Phys **115(14):** 143902 (2014).

[16] Y. Li, J. R. Sun, J. Zhang, and B. G. Shen, J. Appl. Phys **116(4):** 043916 (2014).

[17] S. EI. Helali, K. Daoudi, A. Fouzri, M. Oumezzine, M. Oueslati, and T. Tsuchiya, Appl. Phys. A **108,** 379-384 (2012).

[18] M. Bibes, LI. Balcells, S. Valencia, S. Sena, B. Martinez, and J. Fontcuberta, J. Appl. Phys **89(11),**6686-6688 (2001).

[19] S. Valencia, LI. Balcells, B. Martinez, and J. Fontcuberta, J. Appl. Phys **93(10),**8059-8061 (2003).

[20] He Wang, Lvkang Shen, Tingzhi Duan, Chunrui Ma, Cuimei Cao, Chanjun Jiang, Xiaoli Lu, Huiyuan Sun, and Ming Liu, ACS Appl. Mater. & Interfaces **11**, 22677-22683 (2019).

[21] Jijie Huang, Han Wang, Xing Sun, Xinghang Zhang, and Haiyan Wang, ACS Appl. Mater. & Interfaces **10,** 42698-42705 (2018).

[22] S. S. Hong, M. Q. Gu, M. Verma, V. Harbola, B. Y. Wang, Di Lu, A. Vailionis, Y. Hikita, R. Pentcheva, J. M. Rondinelli, and et al, Science **368,** 71-76 (2020).

[23] P. Mandal, B. Bandyopadhyay, and B. Ghosh, Phys. Rev. B **64**, 607-611 (2001).

[24] Songbin Li, Chuanbin Wang, Qiang Shen, and Lianmeng Zhang, Vacuum **164**, 312-318 (2019).

[25] C. Sen, E. Dagotto, Phys. Rev. B **102**, 035126 (2020).

[26] M. Viret, L. Ranno, and J. M. D. Coey, Phys. Rev. Lett. **75**, 3910-3913 (1997).

[27] S. B. Li, C. B. Wang, D. Q. Zhou, H. X. Liu, L. Li, Q. Shen, and L. M. Zhang, Ceram. Int. **44,** 550-555 (2018).

[28] P. K. Siwach, H. K. Singh, and O. N. Srivastava, J. Phys.: Condens. Matter **18**, 9783-9794 (2006).

[29] C. R. Ma, M. Liu, J. Liu, G. Collins, Y. M. Zhang, H. B. Wang, C. I. Chen, Y. Lin, J. He, J. C. Jiang, and et al, ACS Appl. Mater. & Interfaces **6,** 2540-2545 (2014).

Table 1. The VRH characteristic temperature and average nearest-neighbor hopping distance R of different tensile or compressive strain derived from the resistivity of LCMO as function of temperature at 0 T and 9 T.

$\rho = \rho_0 \times e^{(\frac{T_0}{T})^{\frac{1}{4}}}$	Tensile				Compressive			
	0 T		9 T		0 T		9 T	
strain	T_0 (10^7 K)	R (Å)	T_0 (10^7 K)	R (Å)	T_0 (10^7 K)	R (Å)	T_0 (10^7 K)	R (Å)
0	6.82	12.30	1.4	14.03	6.82	12.30	1.4	14.03
0.4%	7.23	12.24	1.76	13.77	9.33	11.98	3.3	13.07
0.8%	9.47	11.96	2.57	13.34	9.08	12.02	2.46	13.39
1.33%	10.63	11.84	3.63	12.97	12.91	11.65	4.28	12.79

Figure Captions:

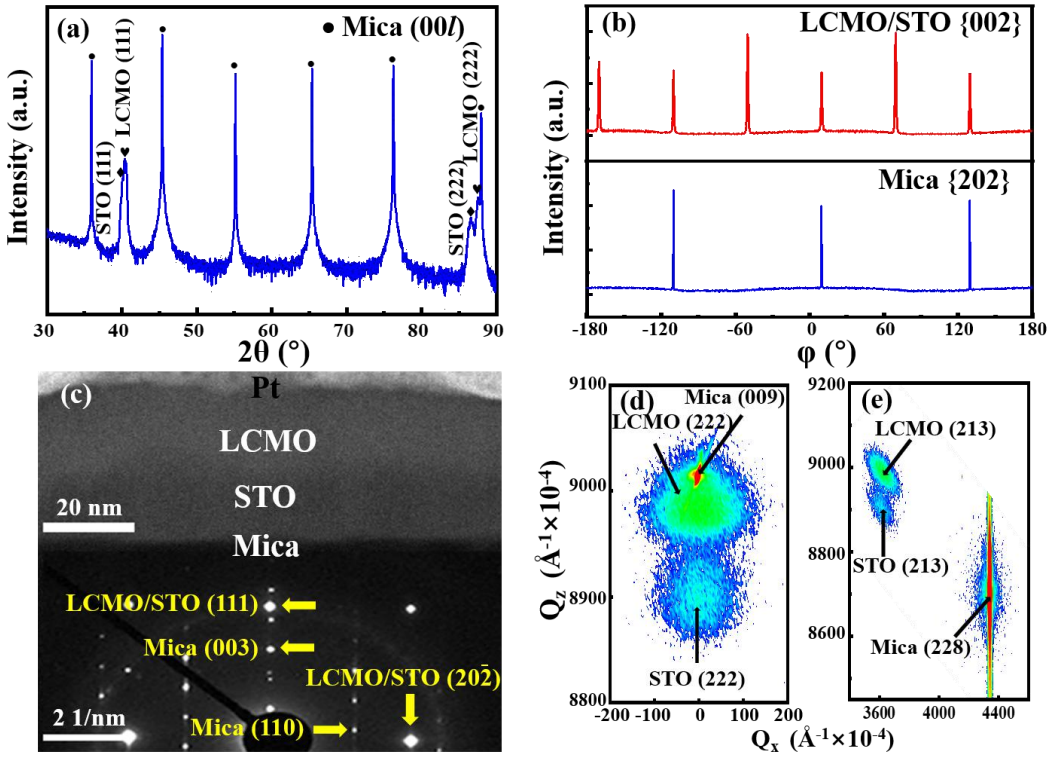

Figure 1. (a) XRD *θ-2θ* pattern of LCMO thin film and STO buffer layers on (001) F-Mica substrate. (b) The φ scans taken around the {202} reflections of F-Mica and {002} reflections of LCMO/STO, respectively. (c) The TEM image of a cross-section sample and the SAED patterns taken from the areas covering the interfaces between the films and substrate. (d) RSMs taken around the symmetric (222) of the LCMO thin film. (e) RSMs taken around asymmetric (213) reflections of the F-Mica substrate.

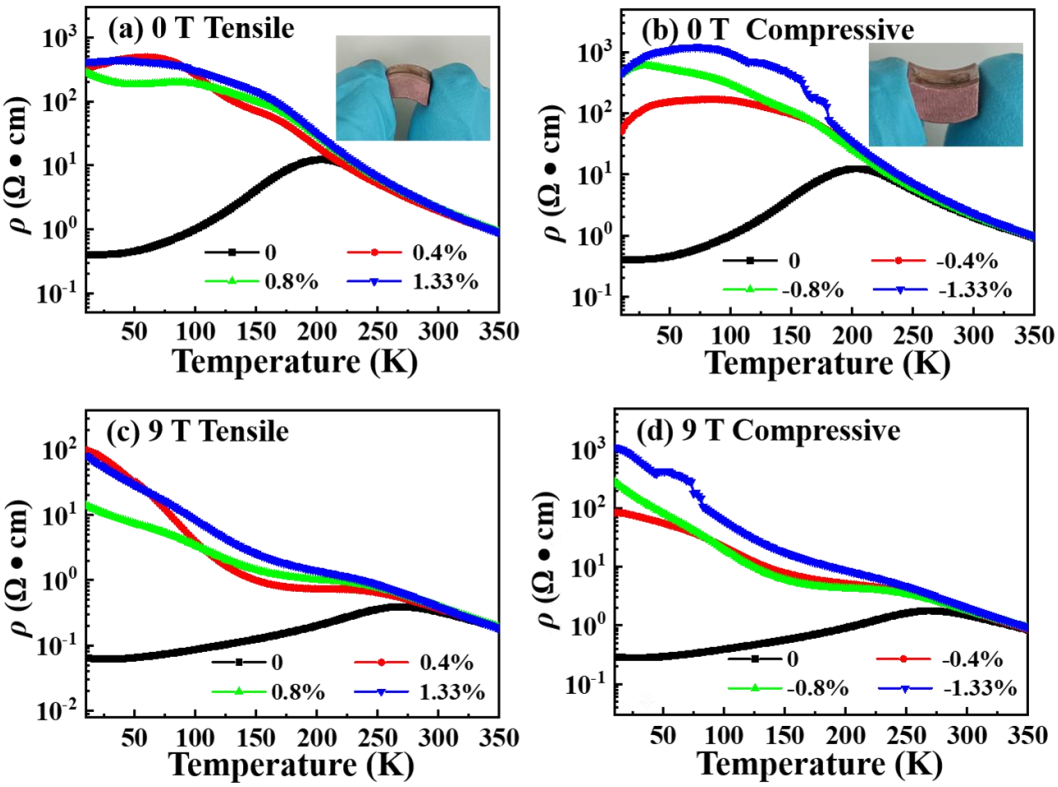

Figure 2. Transport properties of the flexible LCMO thin film under extra mechanical tensile and compressive strain induced by convex and concave bending without magnetic field (a, b) and with 9 T magnetic field (c, d).

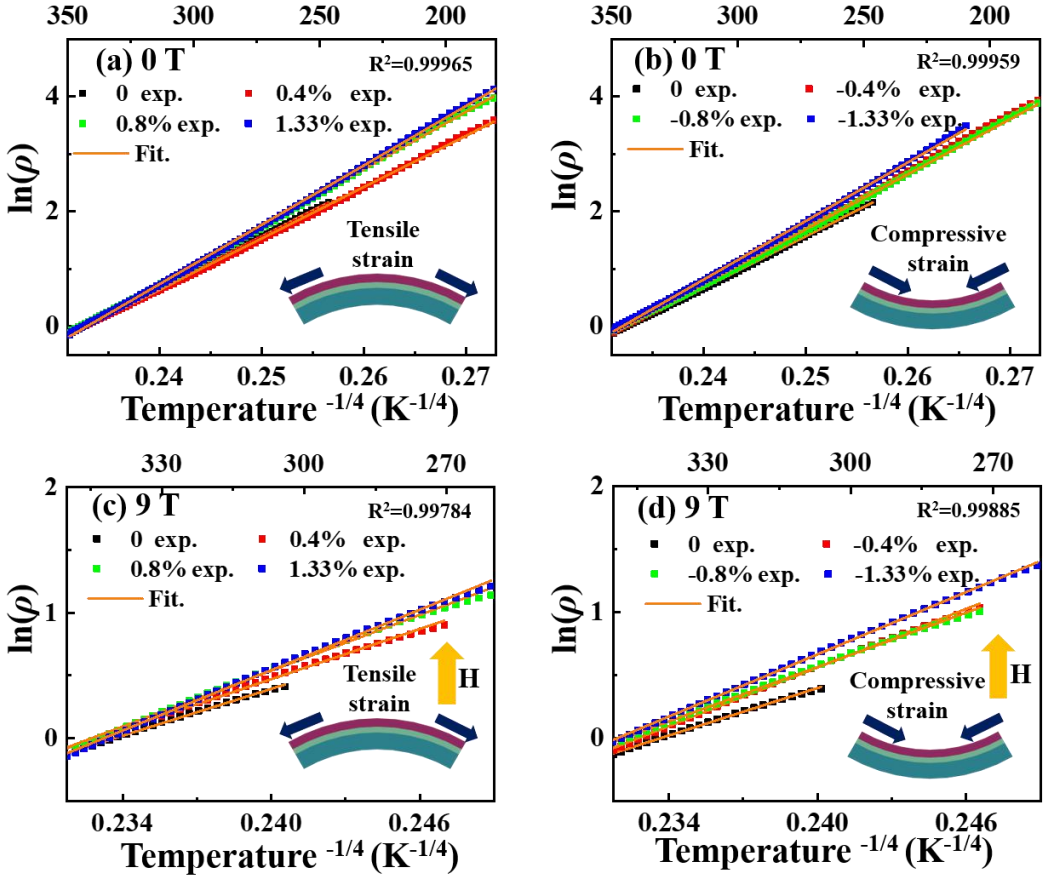

Figure 3. Logarithm of the resistivity versus $T^{-1/4}$ plot of the LCMO thin film under extra tensile and compressive strain induced by various bending curvature radii above the transition temperature at 0 T (a, b) and 9 T (c, d).

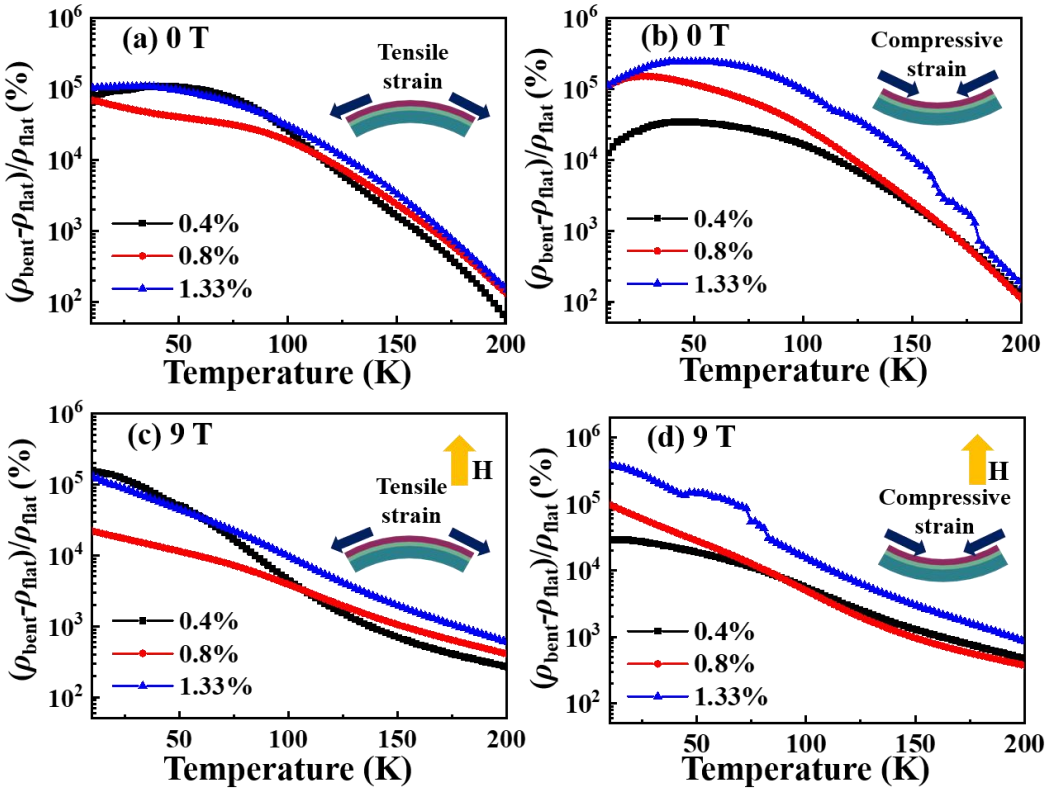

Figure 4. Resistivity change ratio between the LCMO thin films under tensile and compressive strain and no extra strain at 0 T (a, b) and 9 T (c, d).